Nanoscale

PAPER

View Article Online
View Journal | View Issue





Cite this: *Nanoscale*, 2020, **12**, 13119

# Adsorption and ordering of amphiphilic rod–coil block copolymers on a substrate: conditions for well-aligned stripe nanopatterns†

Liquan Wang, ‡ Zhengmin Tang,‡ Da Li, Jiaping Lin * and Zhou Guan

Received 13th February 2020,
Accepted 10th June 2020

DOI: 10.1039/d0nr01244k

rsc.li/nanoscale

Controlling the ordering of self-assembled nanostructures is vital in block copolymer nanotechnology but still presents a challenge. Here we demonstrated that the adsorption and ordering of amphiphilic rod–coil block copolymers on a substrate can generate well-aligned stripe nanopatterns by dissipative particle dynamics simulations. The effects of the copolymer concentration and the surface affinity on the formation of stripe nanopatterns were examined. The simulation results revealed that the well-aligned stripe nanopatterns with controllable thickness and stripe width can be obtained in the systems with higher copolymer concentration and surface affinity. An immersion coating experiment was designed to verify the simulation results, and an agreement is shown. The present work provides a strategy for constructing well-aligned stripe nanopatterns in a controllable way.

## 1. Introduction

Thin films of block copolymers have attracted considerable research interest due to their potential applications in emerging nanotechnologies such as ultrahigh-density storage media,[1] nanoporous membrane,[2,3] and nanolithography.[4] Plenty of these applications require the use of thin films in geometries of high precision and well-defined orientations. Various techniques have been employed to guide the self-assembly of block copolymers in thin films, including solvent annealing,[5,6] graphoepitaxy,[7,8] chemical pre-patterning,[9–11] and external fields such as mechanical flow fields,[12,13] electric fields,[14,15] magnetic fields,[16,17] and thermal gradients.[18] However, the ability of these technologies to control ordering in block copolymer thin films still needs to be improved to meet the requirements of next-generation thin films.

Self-assembly of block copolymers on an unpatterned substrate generally leads to localized ordering into polycrystalline-type structures with numerous grain boundaries.[19] This limits the utility of block copolymers in the fields that require both domain orientation and long-range order. Graphoepitaxy and chemical pre-patterning are two conventional approaches to direct block copolymer self-assembly in an attempt to overcome this inherent deficiency of copolymer assembly.[7] The research efforts have demonstrated that periodic patterns of parallel lines,[20] close-packed dots,[21] and more complex structures such as concentric rings[22] and bent lines[23] can be generated using these two approaches. However, these approaches require initial substrate patterning by photolithography to create ordered topographical features of block copolymers. This additional step significantly increases the cost and time requirements for the arrangement of block copolymers.[24]

The adsorption and ordering of amphiphilic rod–coil block copolymers onto the surface of the substrate can be a promising method for thin films with controlled domain ordering. The liquid crystalline aligning interactions between rod blocks can facilitate the formation of well-aligned nanostructures.[25,26] However, it is a challenge to access long-range order in rod–coil block copolymer films because rod blocks usually have high melting temperatures and a strong tendency to crystallize. One of the methods to access well-aligned structures is air–liquid interfacial self-assembly of rod–coil block copolymers.[27–29] In addition to the rigid nature of rod blocks and the block copolymer architecture, the fluidic nature of the air–water interface is helpful for the formation of well-aligned structures.

In contrast with the fluidic interface, the immersion coating method could generate well-aligned patterns on a solid substrate.[25] To date, there are many works regarding the preparation of thin films from the immersion coating of rod–coil block copolymers on the substrate.[25,30–33] In these works, however, the copolymers are usually chemically bonded to the

*Shanghai Key Laboratory of Advanced Polymeric Materials, Key Laboratory for Ultrafine Materials of Ministry of Education, School of Materials Science and Engineering, East China University of Science and Technology, Shanghai 200237, China. E-mail: jlin@ecust.edu.cn*

†Electronic supplementary information (ESI) available: Simulation method, experimental method, and effect of copolymer concentration and surface affinity on the morphologies. See DOI: 10.1039/d0nr01244k

‡These authors contributed equally to this work.

substrate, which causes the disordered surface pattern to yield. Therefore, whether or not the immersion coating of rod–coil block copolymers that are not anchored to the substrate can generate thin films with controlled thickness and domain order remains a question. Moreover, how the rod–coil block copolymers are adsorbed and ordered on the substrate needs to be addressed.

The amphiphilic copolymers can be irreversibly adsorbed on the substrate as the copolymer concentration is low, while the assembly behaviors of amphiphilic copolymers on the substrates are dictated by the interplay between the adsorption and micellization in bulk solution (*i.e.*, the solution excluding the substrate) as the polymer concentration is high.[34,35] The interplay is influenced by various thermodynamic parameters such as the concentration of the copolymers and the surface affinity to the copolymers. Distinct balances have to be achieved under each condition, which renders the systems much complicated. Theory and simulations such as Flory-type approximation and Monte Carlo simulations were employed to understand the behaviors and explore the structures of the films formed by block copolymers.[34] Recent works, however, are mainly concentrated on the coil–coil block copolymers, and less attention is paid to the rod–coil block copolymer systems. The capability of the amphiphilic rod–coil block copolymers to generate well-aligned patterns on the substrate remains to be explored.

In this work, we performed dissipative particle dynamics (DPD) simulations of a coarse-grained model to systematically explore the adsorption and ordering behaviors of the amphiphilic rod–coil copolymers on a substrate. It was demonstrated that the rod–coil block copolymers could self-assemble into well-aligned stripe nanopatterns with a fixed thickness on the substrate as the copolymer concentration and the surface affinity are high. Guided by the predictions from the DPD simulations, we conducted a designed experiment of solution self-assembly of poly($\gamma$-benzyl L-glutamate)-*b*-poly(ethylene glycol) (PBLG-*b*-PEG) on the silicon wafer covered with polystyrene. It was found that the experimental observations well support the simulation results. We believe that the present approach could be a new route to produce thin films with well-aligned patterns and controlled thickness.

## 2. Simulation methods

We considered a solution system consisting of amphiphilic rod–coil diblock copolymers, solvents, and a flat substrate. Dissipative particle dynamics (DPD), a simulation technique for hydrodynamics behavior, was employed for the present study. The DPD method was introduced by Hoogerbrugge and Koelman and was reformulated by Español and Warren as a proper statistical mechanics model.[36–40] For details of the method, see section 1.1 of the ESI.† The model used in the dissipative particle dynamics (DPD) simulations is schematically illustrated in Fig. 1a. As shown in the figure, the copolymers are coarse-grained into two kinds of DPD beads with neighboring ones connected by harmonic spring potentials. Angle interaction between triplets of DPD beads was applied to one of the blocks (green) to control the rigidity of the polymer chains. The remainder beads (red) in the copolymers are assigned to the flexible chains. Each rod (or coil) block consists of four beads. The solvents are modeled by individual DPD beads (not shown in Fig. 1a). A solid flat substrate with two surfaces being different affinities is placed at the bottom of the simulation box. We constructed the flat substrate by arranging the DPD beads in the FCC packing fashion. The beads are packed close enough (the minimum bead-to-bead distance is $0.4r_c$) to prevent the copolymers and solvents from permeating through the flat substrate. As the beads are packed tightly, the packing manner could have a less marked effect on the simulation results (see Fig. S4†).

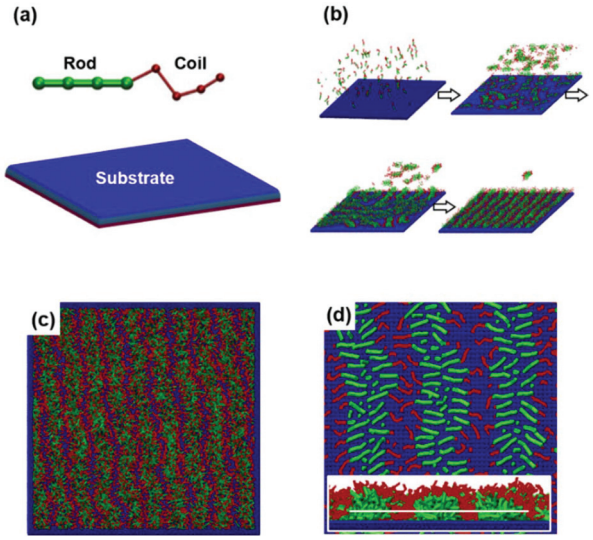


**Fig. 1** (a) Schematic of the simulation system consisting of rod–coil block copolymers and a flat substrate. (b) Sketch of the adsorption and ordering of rod–coil block copolymers on the substrate. (c) Top-view of the simulation structures on the substrate. (d) Cross-section of the stripe pattern on the substrate. The white line in insert indicates the position where the cross-section creates.

The interaction parameters $a_{ij}$ between different types of beads were given in Table 1. Note that in the DPD method, there is a linear relationship between the Flory–Huggins parameter $\chi_{ij}$ and the interaction parameters $a_{ij}$. Larger $a_{ij}$ means larger $\chi_{ij}$ and stronger incompatibility between the species i and j. In the work, R, C, S, and P (or P′) denote rod blocks, coil

**Table 1** Interaction parameters $a_{ij}$ between various components

| | R (rod) | C (coil) | S (solvent) |
|---|---|---|---|
| R | 25 | | |
| C | 80 | 25 | |
| S | 80 | 30 | 25 |
| P/P′[a] | $a_{RP}$/120 | $a_{CP}$/120 | 120/120 |

[a] **P** and **P′** represent upper and under surfaces of the substrate, respectively.

blocks, solvents, and the beads constructing the flat substrate, respectively. For the beads of the same species, the repulsive parameters $a_{ij}$ were set to 25. A large value of $a_{RC}$ (= 80) is chosen to represent the incompatibility between rod and coil blocks. The undersurface P′ of the substrate is incompatible with copolymers by setting $a_{RP'} = a_{CP'} = 120$, while the upper surface P is slightly miscible with copolymers by setting $a_{RP} = a_{CP} < a_{CP'}$. At the beginning of the simulation, the polymers and solvents are initially randomly distributed in the simulation box, and the copolymer and substrate are soluble in solvents ($a_{RS} = a_{CS} = a_{PS} = 25$). We then changed the interaction strengths to mimic the water addition process.[40] The details are given as follows (see Table 1). We set the larger $a_{RS}$ (= 80) than $a_{CS}$ (= 30) to simulate the solvent selectivity to coil blocks. Also, both two surfaces of the flat substrate are hydrophobic by setting $a_{PS} = 120$.

The simulations were performed in the $l \times l \times h$ three-dimensional spaces with periodic boundary conditions. The NVT ensemble was adopted in the simulation. The size of the flat substrate is $l \times l \times 1$. The total number of the DPD beads of polymers and solvents can thus be calculated as $l^2 \times (h - 1) \times \rho$, where $\rho = 3$ is the number density of the system. In this work, we chose $l$ and $h$ to be $50r_c$ and $10r_c$, respectively. Therefore, the number of DPD beads for polymers and solvents is 67 500. The velocities with Gaussian distributions are applied to all of the beads except those forming the flat substrate. The DPD simulations are run at least for $30000\tau$ to achieve the equilibrium of the self-assembly. The time step was set as $\Delta t = 0.01\tau$, where $\tau$ is the unit of time. The units of mass, length, and energy are defined by $m$, $r_c$, and $k_BT$, respectively. For each case, we conducted the simulations with various random number seeds for ten times. The final quantitative results were averaged over the ten simulations.

## 3. Results and discussion

The present work mainly focuses on the dissipative particle dynamics (DPD) simulations of an immersion coating process. In this coating process, as sketched in Fig. 1b, a flat substrate is immersed into a solution consisting of amphiphilic rod–coil diblock copolymers and common solvents. As the selective solvents are added, the rod–coil block copolymers can be adsorbed on the surface of the substrate. Simultaneously, the rod–coil block copolymers are gradually rearranged, and surface patterns are finally formed.

In Fig. 1c, we presented a characteristic pattern of the thin film, which is formed by the self-assembly of the amphiphilic rod–coil block copolymers on the upper surface of the substrate. A highly ordered stripe nanopattern without defects was observed. The hydrophobic rod blocks are packed orderly to form the inner parts of the stripes, whereas the hydrophilic coil blocks connected with one end of rod blocks extend into the solution to form the shell. Under this circumstance, the coil blocks can enwrap the rod block cores to stabilize the structures. Fig. 1d shows that the rod blocks are almost perpendicular to the long axis of the stripes and parallel to the substrate. From the cross-section shown in the insert of Fig. 1d, it is evident that the structures of the stripes are semi-cylinders. These results demonstrate that the rod–coil block copolymers are capable of self-assembling into well-aligned patterns on the substrates. To understand the condition for the formation of well-aligned stripes, we conducted a systematical investigation on the effect of copolymer concentration and surface affinity (see details below).

### 3.1. Adsorption of copolymers on substrate

In the solutions, the copolymers can be either absorbed on the substrate or dispersed in the bulk solution. In the bulk solution, micelles are formed as the polymer concentration exceeds critical micelle concentration. Note that the bulk solution here represents the region where the substrate and the adsorbed layer are excluded.

The copolymers can be irreversibly adsorbed on the surface of substrates as long as the surface is not saturated. This is because the adsorption of copolymers on the substrate can reduce the total free energy of the systems. After saturation, the surface of the substrate is then in equilibrium with the bulk solution by exchanging copolymers between the thin film attached to the substrate and the micelles in bulk solution.

To understand the above behavior, we examined the density distribution of block copolymers along the direction $z$ normal to the substrate. Note that the density is the averaged over the $x$–$y$ plane for various times. The result is presented in Fig. 2a. As shown, the density profile shows a peak around $z = 1.1r_c$, and a depletion layer (I) exists in the range of $z < 1.1r_c$. The depletion layer (I) is a region where the copolymers are distributed away from the substrate. Because the depletion layer (I)

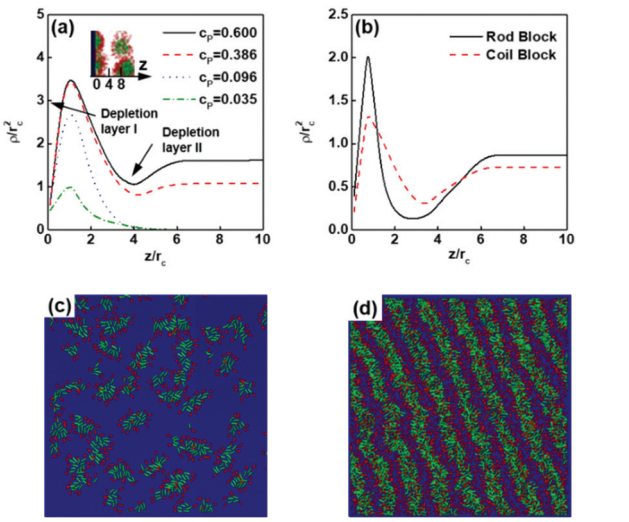


Fig. 2 (a) Density of rod–coil block copolymers along $z$-axis normal to the substrate for the systems with various copolymer concentration $c_p$, where the interaction strength is $a_{RP} = a_{CP} = 30$. (b) Density of rod blocks and coil blocks along $z$-axis for the system with $c_p = 0.217$ and $a_{RP} = a_{CP} = 30$. Representative simulation structures on the substrate obtained at (c) $c_p = 0.035$ and (d) $c_p = 0.386$, where $a_{RP} = a_{CP} = 30$.

originates from the repulsion between the substrate and the segments of the copolymers, the positions of the peaks remain nearly unchanged with the change of the copolymer concentration. At lower copolymer concentration, the density of the copolymers far away from the substrate is zero, implies that there are no free copolymers in the bulk solution. As the concentration of the copolymers increases, the density of the copolymers shows an increase, but the density near the substrate is unchanged at higher copolymer concentration. There is another depletion layer (II) between the film and the bulk solution. This depletion layer (II) becomes marked upon increasing the copolymer concentration. Since the position of the depletion layer fluctuated along the plane of the laterally structured film, the statistically average density is not "depleted" entirely in contrast with the depletion layer (I). Despite this, it signals that the non-adsorbing copolymers are prevented from merging with the adsorbed film. The depletion layer (II) can be visible by plotting the density distribution of rod blocks and coil blocks, respectively. The result is given in Fig. 2b. As shown, the rod blocks are completely depleted in the depletion layer (II).

The copolymer concentration not only has a pronounced influence on the adsorption of copolymers on the substrate but also affects the structures of absorbing layers. Fig. 2c and d show two typical morphologies of the thin films obtained at lower copolymer concentration ($c_p$ = 0.035) and higher copolymer concentration ($c_p$ = 0.386), respectively. One can see that as the copolymer concentration is low, the copolymers are more likely to form surface micelles, that is, small spherical aggregates and short stripes on the substrate. When the copolymer concentration is high, the ordered stripe patterns appear on the substrate.

The number of copolymers absorbed on the substrate can be further evaluated by examining the density of the copolymers in thin films. In Fig. 3a, we plotted the corresponding density as a function of the copolymer concentration. The density of the copolymers dispersed in bulk solution was also given in the figure. As the copolymer concentration is lower than 0.18, the density of copolymers on the substrate increases linearly, but that in solution remains vanishingly small. It indicates that the copolymers are almost adsorbed onto the substrate to form films. As the copolymer concentration is higher than 0.2, the density of the copolymers on the substrate remains constant, and that in bulk shows a linear increase. Under this condition, the amount of copolymers absorbed on the substrate reaches a saturation value of *ca.* 3.5. The saturation value is slightly larger than the average density of 3. Such a saturation characteristic is also reflected by the variation of film thickness as a function of the copolymer concentration, which is shown in Fig. 3b. It can be seen that for various $a_{RP}$ values, the film thickness first increases and then keeps unchanged with increasing the copolymer concentration.

In addition to the copolymer concentration, the adsorption behavior is also dependent on the surface affinity to the copolymers. The surface affinity can be tuned by changing the value of $a_{RP}$ in the simulation (we have set $a_{RP} = a_{CP}$ for simplicity). The smaller value of $a_{RP}$ represents the higher surface affinity to the copolymers. Fig. 3c and d show the density of the copolymers absorbed on the substrate and the film thickness as a function of the value of $a_{RP}$, respectively. As shown, for various values of $c_P$, the film density decreases, and the film thickness increases with increasing the $a_{RP}$ value. Increasing the surface affinity leads to the adsorption of more copolymers on the substrate before saturation. As the $c_P$ increases, the adsorption is saturated at higher $a_{RP}$ value (lower surface affinity). However, understanding the relationship between film thickness and surface affinity is not intuitive. This is related to the structure of the stripes, which is discussed in the following section.

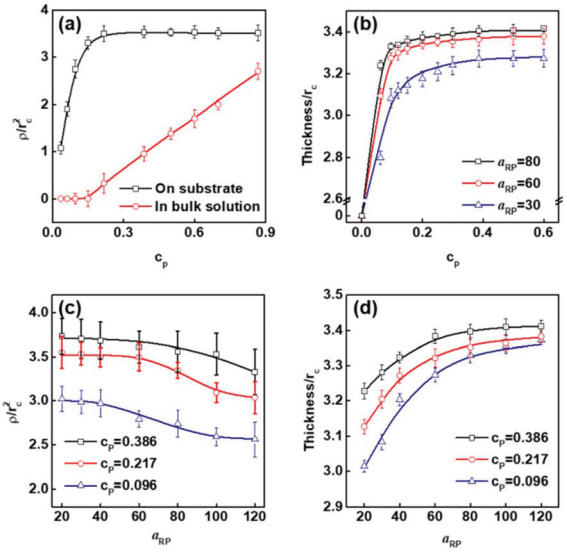


Fig. 3 (a) Density of rod–coil block copolymers absorbed on the substrate and dispersed in bulk solution as a function of the copolymer concentration $c_p$, where $a_{RP} = a_{CP} = 30$. (b) The thickness of the stripes as a function of $c_p$. (c) The density of the copolymer absorbed on the substrate as a function of the interaction strength $a_{RP}$. (d) The thickness of the stripes as a function of the $a_{RP}$.

### 3.2. Structure and ordering of stripe nanopatterns

Of particular interest is the formation of the stripe nanopatterns as the rod–coil block copolymers are attracted to the substrate. This subsection focuses on the structure of the stripe nanopatterns. To examine the ordering of the stripe patterns, we adopted our previous method to calculate the in-plane orientation distribution of the stripes and the order parameter of the patterns (the details regarding the calculation of order parameters are given in section 1.2 of the ESI†).[41,42] The local tangent vectors along the interfaces between the domains rich in rod and coil blocks are obtained by averaging the out-of-plane density. The angle between the tangent vector and the director, denoted as $\alpha$, is used to characterize the local orientation distribution of the cylinders (see the inset of Fig. 4a). Fig. 4a shows the distribution of the $\alpha$ angle. It can be seen that the angles show a peak at $\alpha$ = 0 and are symmetrically dis-

 

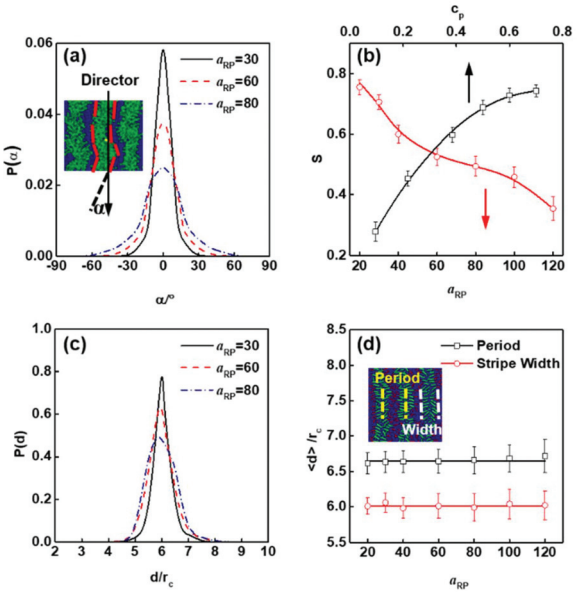


Fig. 4 (a) Distribution of the orientation angle $\alpha$ of the stripes relative to the director, where $c_p$ = 0.386. The insert shows the definition of the angle $\alpha$. (b) Order parameter $S$ of the stripes as a function of $a_{RP}$ (red line, $c_p$ = 0.386) and $c_p$ (black line, $a_{RP}$ = 30), respectively. (c) Distribution of the stripe width for the system with various $a_{RP}$, where $c_p$ = 0.386. (d) The average stripe width and average in-plane period of the films as a function of $a_{RP}$, where $c_p$ = 0.386.

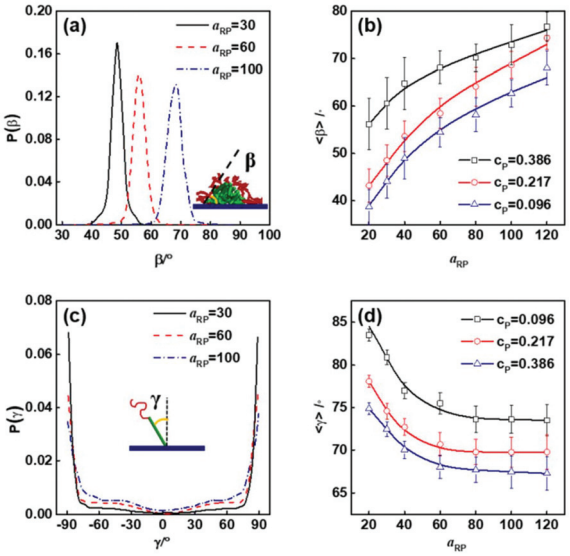


Fig. 5 (a) Distribution of the contact angle $\beta$ for the systems with various values of $a_{RP}$, where $c_p$ = 0.386. The insert shows the definition of the angle $\beta$. (b) Average contact angle $\langle\beta\rangle$ as a function of $a_{RP}$. (c) Distribution of orientation angle $\gamma$ for rod blocks, where $c_p$ = 0.386. The insert shows the definition of the angle $\gamma$. (d) Average orientation angle $\langle\gamma\rangle$ for rod blocks as a function of $a_{RP}$.

tributed around $\alpha$ = 0. As the $a_{RP}$ value increases, the distribution of $\alpha$ angles broadens.

To quantitatively measure the order of patterns on the substrate, we used the order parameter $S$ to describe the order degree of the stripe alignment. As the order parameter $S$ approaches one, perfectly ordered patterns are generated. In Fig. 4b, black and red lines show the order parameter $S$ as a function of the copolymer concentrations $c_p$ and the interaction strength $a_{RP}$, respectively. One can see that the order parameter $S$ increases as either the $a_{RP}$ value decreases or the copolymer concentration increases. The order parameters are higher than 0.7 as the $a_{RP}$ value is lower than 25 or as the copolymer concentration increases beyond 0.5, indicating that the stripe patterns at these conditions are well-aligned.

Fig. 4c shows the distributions of the stripe width of the films. As shown in Fig. 4c, the distribution of stripe width is symmetrical around $d = 6r_c$ and becomes wide upon increasing the $a_{RP}$ value. The average stripe width and average in-plane period were also statistically analyzed. The results are shown in Fig. 4d. As shown, the average stripe width, which is roughly $6r_c$, is nearly independent of the $a_{RP}$ values. The in-plane period of the stripes is also unchanged as the $a_{RP}$ value varies. The in-plane period is only slightly larger than the stripe width, implying that the stripes are highly asymmetric. Such a structure is different from the widely studied lamellae where the period is usually twice the layer width.[43]

The stripe nanopattern, different from the lamellae, is a parallel arrangement of semi-cylinders (see the cross-section shown in the inset of Fig. 1c). We used a contact angle $\beta$ to characterize the cross-section of the semi-cylinders. The contact angle, related to the wetting behaviors of the semi-cylinders, is defined as the angle between the tangent to the core and the substrate (see the inset of Fig. 5a). Fig. 5a shows the distributions of the contact angle at various values of $a_{RP}$. With increasing the $a_{RP}$ values, the distribution shifts towards the higher value of the contact angle and becomes wide. This is reflected by the variation of the average contact angle as a function of the $a_{RP}$ values, which is shown in Fig. 5b. As shown, the average contact angle increases as the $a_{RP}$ value increases. This tendency becomes less marked as the copolymer concentration increases. The result can be used to explain the relationship between the film thickness and surface affinity (see Fig. 3d). As the $a_{RP}$ decreases, the copolymers are attached to the substrate more closely, and the contact angle of stripes decreases, leading to a decrease in the film thickness.

The wetting behavior of the stripes is closely associated with the orientation of the rod blocks of the rod–coil block copolymers. Here, we chose the angle $\gamma$ between the rod blocks and the direction normal to the substrate to characterize the orientation of the rod blocks within the cross-section of the cylinders (see the inset of Fig. 5c). Fig. 5c shows the distribution of the $\gamma$ angles. The peak of the distribution appears at 90°, implying that the rod blocks tend to lie on the substrate. The distribution becomes broad as the $a_{RP}$ value increases. In Fig. 5d, we plotted the average orientation angle as a function of the $a_{RP}$ value. As shown, the average orientation angle decreases with increasing the $a_{RP}$ value and increases as the copolymer concentration decreases. Such variations result from the balance of orientation entropy of the rod blocks and

the interaction energy between rod blocks and substrate. The orientation entropy favors the "lying down" packing of rod blocks on the substrate. However, the repulsion between rod blocks and substrate drives the "standing up" arrangement of rod blocks on the substrate to reduce the unfavorable interaction enthalpy effectively. The interplay of these two effects results in the decrease of average orientation angle as the interaction $a_{RP}$ between rod blocks and substrate increases.

To fully understand the adsorption and ordering behaviors of the amphiphilic rod–coil block copolymers on the substrate, we summarize the observed morphologies into a stability region diagram. The stable morphology diagram is shown in Fig. 6. The diagram consists of three regions. They are surface micelles (spherical micelles or short stripes attached to the surface of the substrate), surface stripes (long stripes attached to the surface of the substrate), and surface stripes with micelles dispersed in bulk solution (for a direct view of the morphologies, see Fig. S3 and S4†). In the diagram, the red, yellow, green, and blue symbols represent surface micelle, surface stripes, surface stripes with micelles dispersed, and well-aligned surface stripes with micelle dispersed, respectively. When the copolymer concentration is low and the surface affinity is high, the copolymers are almost absorbed by the substrate and form surface micelles of spherical shape. The surface stripes without micelles dispersed in bulk solution are mainly observed for the systems with intermediate concentration and high surface affinity. When the copolymer concentration is high, the amount of stripe-forming copolymers reaches the saturation value, and the excess copolymers self-assemble into the micelles in bulk solution. As shown in the figure, the stripes in the region below the dashed line are well-aligned, where the $S$ is higher than *ca.* 0.6. The diagram shows that the condition for the amphiphilic rod–coil block copolymers to form a well-aligned stripe pattern is higher copolymer concentration and higher surface affinity.

The transformation from surface micelle of spheres or short cylinders to stripe nanopatterns with increasing $a_{RP}$ is related to the interfacial energy. Note that we have assumed that $a_{RP} = a_{CP}$ in the study. As the $a_{RP}$ is low, the incompatibility between rod–coil block copolymer and the substrate is weak, and therefore the copolymers can self-assemble into spherical or short rod micelles having high specific surfaces with the substrate. As the $a_{RP}$ increases, the block copolymers become more incompatible with the substrate. As a result, the rod–coil block copolymers form aggregates with a lower specific surface, such as stripe nanopatterns, in order to reduce the unfavorable interface between the block copolymer and the substrate and further minimize the total free energy.

### 3.3. Dynamics of the formation of stripe nanopatterns

The well-aligned patterns are obtained from the ordering of the rod–coil block copolymers on the substrate. Therefore, we paid attention to the formation process of the stripe patterns. Fig. 7a–c present the simulation morphologies running for $200\tau$, $3000\tau$, and $17000\tau$, respectively. The morphology at the time of $200\tau$ indicates that the rod–coil diblock copolymers are adsorbed on the substrate and form stripes within a short time. The structures at this stage lack order and exhibit a fingerprint feature with a large number of defects. As the self-assembly proceeds, the stripes become more regular, and the defects gradually disappear (see Fig. 7b). At the time of $17000\tau$, well-aligned stripe patterns are obtained by eliminating all the defects.

The defects in the ordering process include two types, that is, disclinations and dislocations. The disclinations consist of +1/2 disclinations (the stripes are rotated 180°) and −1/2 disclinations (three stripes are rotated 120°).[44] The +1/2 disclinations and −1/2 disclinations usually appear as a pair. For the dislocations, one of the parallel stripes is abruptly truncated, and a free end is produced. Fig. 7d–f illustrate the typical elimination of a pair of disclinations in the process. As shown, a

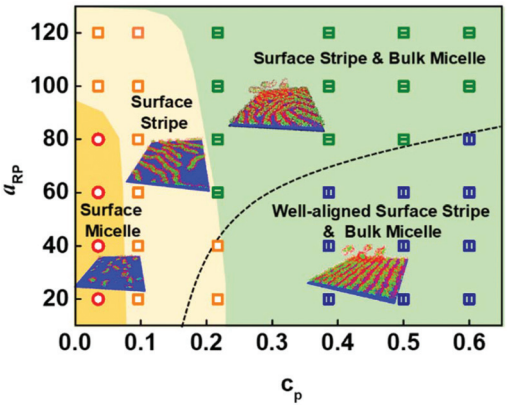


Fig. 6 Morphology diagram in the space of $a_{RP}$ *versus* $c_p$. The red, yellow, green, and blue symbols represent surface micelle, surface stripe, surface stripe with bulk micelle (micelle dispersed in solution), and ordered surface stripe with bulk micelle, respectively. The stripes in the region below the dashed line are well-aligned, where the order parameter is higher than 0.6.

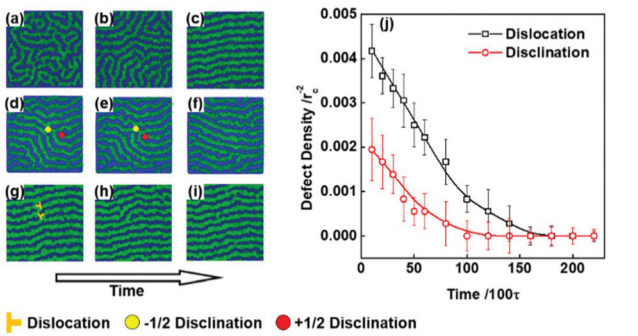


Fig. 7 Morphologies of rod–coil block copolymers on the substrate at the simulation time of (a) $200\tau$, (b) $3000\tau$, and (c) $17000\tau$. (d–f) Representative elimination of a pair of disclinations. (g–i) Representative elimination of dislocations. The simulation times for (d), (e), and (f) are $5000\tau$, $7000\tau$, and $10000\tau$, respectively. The simulation times for (g), (h), and (i) are $13000\tau$, $14000\tau$, and $15000\tau$, respectively. (j) The density of dislocation and disclination as a function of simulation time. The simulation parameter are $a_{RP} = 30$ and $c_p = 0.386$.

+1/2 disclination and a −1/2 disclination close to each other and annihilate together during the ordering process. The representative elimination of dislocations can be seen in Fig. 7g–i. Two dislocations merge and eliminate to form regular stripes.

To quantitatively describe the ordering of the stripes on the substrate, we calculate the density of defects at different stages in the simulation. The result is shown in Fig. 7j, where the density of defects is defined as the number of defects per unit area. Since the +1/2 disclination and −1/2 disclination appear in pairs on the flat substrate, we plotted the density variation of two kinds of disclination in the same curve for simplicity. One can see that three types of defects exist at the early stage of the simulation, and their densities are high. As the simulation proceeds, the densities of defects gradually decrease to zero and then remain unchanged.

Both the structural and dynamic studies show that the rod–coil copolymers can form well-aligned stripe patterns on the substrate as the polymer concentration is high enough. In order to understand the role of rod blocks in the self-assembly, we perform additional simulations for the block copolymers containing one block with various rigidities for a comparison. The rigidities can be controlled by the $k_A$ value of the angle forces. Fig. 8a shows the order parameter $S$ of the stripes against $a_{RP}$ for various values of $k_A$. The $k_A = 0$ corresponds to coil–coil block copolymers. As shown, the order parameter $S$ of the stripes shows a decrease with increasing the $a_{RP}$ value. The order parameter for the coil–coil block copolymers is *ca.* 0.3, indicating the stripes formed by coil–coil block copolymers are disordered (the morphology is shown in Fig. 8c). As the $k_A$ value increases, the order parameter $S$ increases dramatically, and the stripe nanopatterns become more well-aligned (see Fig. 8d–f). The results imply that the amphiphilic rod–coil block copolymers show an advantage in preparing well-aligned stripes over coil–coil block copolymers in solution. Fig. 8b shows the average stripe width and average in-plane period as a function of $k_A$ value. With increasing the $k_A$ value, the stripe width and in-plane period first increase and then keep nearly unchanged, implying the stripe width and in-plane period of the thin film are independent of $k_A$ value as the rod blocks are rigid enough.

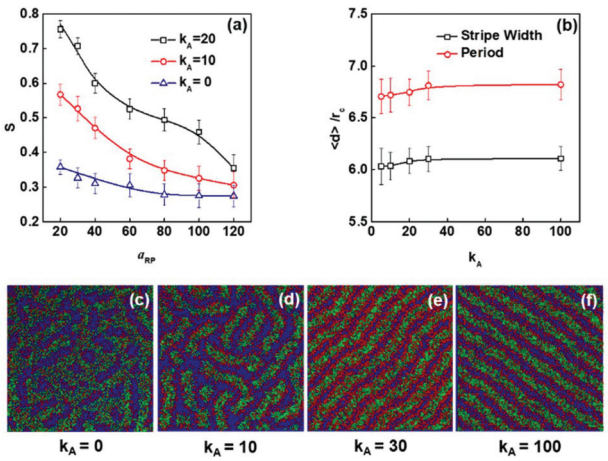


Fig. 8 (a) Order parameter $S$ of the stripes formed by diblock copolymers with various $k_A$ as a function of the interaction strength $a_{RP}$. (b) Plots of average stripe width and average in-plane period of the films as a function of $k_A$ value. Representative morphologies of the films formed by the diblock copolymers with (c) $k_A = 0$, (d) $k_A = 10$, (e) $k_A = 30$, and (f) $k_A = 100$.

### 3.4. Comparison with experimental observations

Several experiments showed that it is hard for coil–coil block copolymers to form highly ordered stripe patterns on a flat substrate without employing sophisticated techniques such as chemical pre-patterning. Lennox *et al.* reported the self-assembly of polystyrene-*b*-poly(2-vinyl pyridine) (PS-*b*-P2VP) coil–coil block copolymers into surface patterns on a Si substrate *via* an immersion coating method where the solvent is toluene.[45] It was found that the surface patterns depend strongly on the copolymer concentration. Stripe patterns are formed at high copolymer concentration. However, the stripe patterns are in disorder. Bazuin *et al.* fabricated thin films of polystyrene-*b*-poly(4-vinyl pyridine) (PS-*b*-P4VP) block copolymers dip-coated from the solutions.[46,47] The stripe patterns with a lower degree of the order were observed for a slower dip-coating rate. (Note that the immersion coating method can be regarded as the dip-coating method with slow dip-coating rate.) These experiments show that the coil–coil block copolymers are ill-suited for producing well-aligned stripe patterns. One the other hand, Park *et al.* reported that the rod–coil block copolymer consisting of a surface-attractive poly(3-triethoxysilylpropyl-isocyanate) (PIC) rod block and a hydrophobic PS coil block readily form regular stripe patterns on the silica surface by the casting method.[25] The PIC blocks pack laterally on the plane in a smectic manner, whereas the PS chains segregate along the ordered PIC chains. This result supports our findings that the rod–coil block copolymers can form well-aligned stripe patterns on the substrate immersed in a solution.

Although Park's casting experiment of PIC-*b*-PS rod–coil block copolymers can somewhat support our simulation results, there still lacks direct evidence about the immersion coating experiments of rod–coil block copolymers. Under the guidance from the DPD simulation results, we designed an immersion coating experiment to prepare well-aligned stripe patterns. In the designed experiment, a poly(γ-benzyl L-glutamate)-*b*-poly(ethylene glycol) (PBLG-*b*-PEG) was used to correspond to the rod–coil block copolymers in simulations, where the PBLG takes an α-helix rigid conformation. The contour lengths of PBLG and PEG can correspond to the DPD model. The block copolymers can self-assemble into lamellar structures in bulks (see section 6 of ESI†). Moreover, silicon wafers covered with polystyrenes (PS-silicon wafer) was prepared and used as the substrate. Note that the DPD is a coarse-grained simulation method, and therefore it is difficult to match the experimental condition and the simulation parameters quantitatively.[48,49]

Fig. 9a shows the schematic of our immersion coating experiment. As shown, the PBLG-*b*-PEG copolymers are first

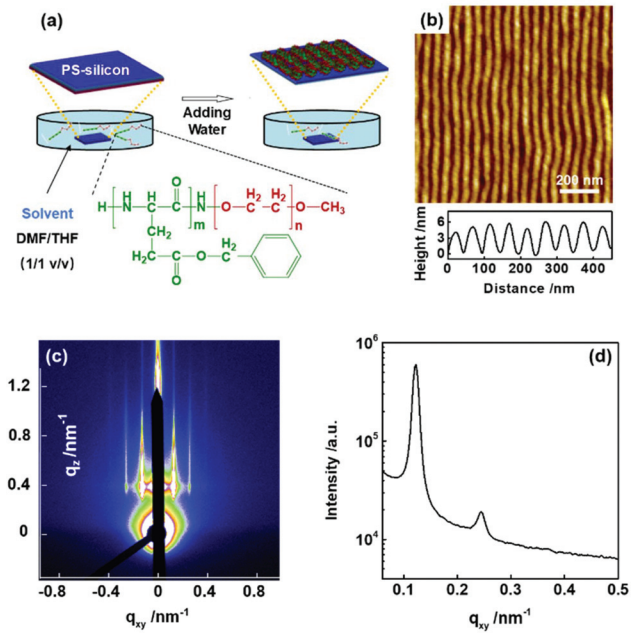


**Fig. 9** (a) Schematic of the self-assembly of PBLG-*b*-PEG on silicon wafers covered with polystyrenes. (b) AFM phase image (the bottom shows the height profile of the stripes), (c) GISAXS pattern, and (d) 1D GISAXS spectra ($q_z$ = 0.4 nm$^{-1}$) of the thin film formed by PBLG-*b*-PEG on the PS-silicon wafer.

dissolved in the mixed solvents consisting of tetrahydrofuran (THF) and *N*,*N*′-dimethylformamide (DMF) (THF/DMF = 1/1 in volume, polymer concentration = 0.4 g L$^{-1}$), and then the PS-silicon wafer was immersed in 3 mL of the polymer solution. Afterward, 1.2 mL of deionized water was added to the polymer solution at a rate of *ca.* 1 mL h$^{-1}$ by an injection pump. After incubation for 2 hours, the wafer was taken out and rinsed with a vast amount of deionized water. (For details of the experiments, see section 2 of the ESI.†) Note that the PS surface of the wafer has a preference for the PBLG-*b*-PEG block copolymers (see section 5 of ESI†), and the concentration of the copolymers is high in the solution. A representative AFM image of the dry sample is shown in Fig. 9b. As can be seen, stripe patterns of PBLG-*b*-PEG block copolymers are formed on the surface of the PS-silicon wafer. The stripe patterns are highly ordered, where the stripes are almost straight and have nearly the same in-plane period of *ca.* 50 nm (see the height profile at the bottom of Fig. 9b). The thickness of the block copolymer film is about 6 nm, implying that the film is a monolayer. The experimental findings further verify the simulation results.

Because the AFM measurements can only provide information about the local surface structure of the thin film, we further characterized the thin film by grazing-incidence small-angle X-ray scattering (GISAXS). The GISAXS can well elucidate the global (both the surface and the bulk) structure of the films.[50] Fig. 9c and d show the corresponding GISAXS data for the entire thin film (the incident angle is 0.3°, which is above the critical angle). The apparent second-order scattering peaks (or spots) can be observed in the GISAXS patterns (see Fig. 9c), indicating that the stripes exhibit a well-aligned periodic in-plane arrangement over a large area in the single-layer film. The first and second peaks are located at $q_{xy}$ = 0.12284 nm$^{-1}$ and $q_{xy}$ = 0.24444 nm$^{-1}$, respectively, and their ratio approaches 1 : 2. The in-plane period is evaluated to be *ca.* 50 nm according to the wave vector of the primary diffraction peak (see Fig. 9d), which is consistent with the period observed in the AFM image (Fig. 9b). To understand how ordering the stripe nanopattern is, we evaluated the correlation length to characterize the grain size in terms of 1D GISAXS spectra (for details, see section 2.5 of ESI†). The correlation length is about 650 nm, which is *ca.* 13 times of the periodicity.

### 3.5. Discussion

Our simulations and designed experiments indicate that the self-assembly of amphiphilic rod–coil copolymers on the flat substrate (*i.e.*, immersion coating method) provides a novel and facile strategy to prepare thin film with controlled structures. Well-aligned patterns of semi-cylinder stripes were predicted for the systems with higher copolymer concentration and surface affinity. Instead of the immersion, the films can also be cast on the substrates.[25] In the casting methods such as the spinning coating method, however, the thickness of the film is dependent on the polymer amount on the substrate, and the defects in the patterns can easily be "frozen" in the annealing process. The present immersion coating method could overcome such drawbacks. Solvent vapor annealing provides an alternative to enhance the ordering of the patterns.[50,51] The vapors can swell the film and increase the chain mobility of the blocks. However, their mobility is very localized and limited once the polymers are cast on the substrates, because the chain exchange between the thin film and the vapors is hindered. In the present method, possible chain exchange exists between the films and the bulk solution (see Fig. 2 and 3). Moreover, the fluidity of liquid crystalline structures can also contribute to the ordered arrangement of rod blocks. Therefore, the rigid polymer chains are much more mobile than those in the solvent vapor annealing method and can assemble into specific structures that minimize the total free energy, as long as the solvents are present.

We noted that the present system could provide a platform for engineering nanostructure with small characteristic sizes (in-plane periods). The traditional lithography techniques based on block copolymers face challenges in generating nanostructured materials with small characteristic sizes.[52] The microphase separation of typical block copolymers is related to chemical incompatibility, *i.e.*, the product of the interaction parameters $\chi$ and the degree of polymerization *N*. For example, the $\chi N$ of symmetric coil–coil block copolymers should be larger than a critical value of *ca.* 10 to induce phase separation.[43] For producing nanostructures with small characteristic sizes, the degree of polymerization should be reduced, and a significantly larger $\chi$ value is required. A large $\chi$ often results from blocks that have disparate interfacial energies. Many

 

researchers have tried their best to increase $\chi$ value by introducing highly incompatible chemical components such as fluorine and inorganic elements.[52,53] Due to the limited choice of highly incompatible components, it is difficult to achieve strong segregation with a sharp interface. In the present system, the entropic loss of rigid blocks could be much smaller than that of coil blocks during the phase separation. As a result, a smaller chemical incompatibility between the rod and coil blocks is sufficient to drive the phase separation.[54,55] For example, the microphase separation between the rod and coil blocks can occur as the $\chi N$ of rod–coil block copolymers (the volume fraction of rod block is 0.5) is larger than *ca.* 5.[55] This value is much smaller than the critical value for the symmetric coil–coil block copolymers. Due to the smaller $\chi N$, the space for choosing chemical components can greatly be expanded, which facilitates the design and generation of nanostructures with small characteristic sizes. Therefore, the entropy-drive self-assembly of rod–coil block copolymers could be a feasible method to produce nanostructures with tiny characteristic sizes.

Moreover, the introduction of selective solvents in the process can help to adjust the chemical incompatibility to induce phase separation. We also note that the in-domain period is slightly larger than the stripe width in the thin films (see Fig. 4d and 8b) due to the highly asymmetric block copolymer system. For traditional self-assembly, only the spot nanopatterns on the substrate can be obtained for highly asymmetric block copolymers.[43] In this work, the combined effects of the solvent swelling of hydrophilic blocks and the orientation interactions of rod blocks result in such highly asymmetric stripe nanopatterns. This asymmetric characteristic is also helpful for the formation of nanostructures with small characteristic sizes.

Well-aligned, laterally structured films on the length scale of copolymers are of interest in a series of applications such as ultrahigh-density storage media,[56,57] nanoporous membranes,[2,3] and nanolithography.[4,58,59] For example, nanoscale stripes can be of practical significance for the microstripe detector, where the silicon stripe detectors have been extensively used for vertex detection and tracking in high-energy physics.[60] In addition to the controllability, the present systems are of diversity in the designs, *i.e.*, various thermodynamic parameters can be tailored to obtain the targeted patterns.

## 4. Conclusions

We employed the dissipative particle dynamics method to simulate the adsorption and ordering of amphiphilic rod–coil block copolymers on the substrate. The influence of the copolymer concentration and the surface affinity on the adsorption and ordering behaviors was investigated. It was found that the rod–coil block copolymers can self-assemble into well-aligned stripe nanopatterns as the copolymer concentration and surface affinity is high enough. The ordering of the stripe nanopatterns can be attributed to the sufficient mobility of the rod–coil block copolymers on the substrate immersed in the solution. The simulation results were found to be consistent with existing experimental findings. Moreover, an immersion coating experiment of PBLG-*b*-PEG was conducted and further demonstrated the validity of the simulation predictions. The present work provides a promising strategy to produce well-aligned stripe patterns with controllable sizes.

## Conflicts of interest

There are no conflicts to declare.

## Acknowledgements

This work was supported by the National Natural Science Foundation of China (21774032, 51833003, 51621002, and 21975073).

## References

1 A. Ethirajan, U. Wiedwald, H. G. Boyen, B. Kern, L. Han, A. Klimmer, F. Weigl, G. Kästle, P. Ziemann, K. Fauth, J. Cai, R. J. Behm, A. Romanyuk, P. Oelhafen, P. Walther, J. Biskupek and U. Kaiser, *Adv. Mater.*, 2010, **19**, 406.
2 D. A. Olson, L. Chen and M. A. Hillmyer, *Chem. Mater.*, 2008, **20**, 869.
3 E. A. Jackson and M. A. Hillmyer, *ACS Nano*, 2010, **4**, 3548.
4 R. Glass, M. Möller and J. P. Spatz, *Nanotechnology*, 2003, **14**, 1153.
5 K. A. Cavicchi, K. J. Berthiaume and T. P. Russell, *Polymer*, 2005, **46**, 11635.
6 Y. S. Jung and C. A. Ross, *Adv. Mater.*, 2009, **21**, 2540.
7 R. A. Segalman, H. Yokoyama and E. J. Kramer, *Adv. Mater.*, 2001, **13**, 1152.
8 V. Mishra, G. H. Fredrickson and E. J. Kramer, *ACS Nano*, 2012, **6**, 2629.
9 Y. Tada, S. Akasaka, H. Yoshida, H. Hasegawa, E. Dobisz, D. Kercher and M. Takenaka, *Macromolecules*, 2008, **41**, 9267.
10 E. Han, I. In, S. M. Park, Y. H. La, Y. Wang, P. F. Nealey and P. Gopalan, *Adv. Mater.*, 2007, **19**, 4448.
11 S. H. Park, D. O. Shin, B. H. Kim, D. K. Yoon, K. Kim, S. Y. Lee, S.-H. Oh, S.-W. Choi, S. C. Jeon and S. O. Kim, *Soft Matter*, 2010, **6**, 120.
12 I. W. Hamley, *J. Phys.: Condens. Matter*, 2001, **13**, R643.
13 A. P. Marencic, P. M. Chaikin and R. A. Register, *Phys. Rev. E: Stat., Nonlinear, Soft Matter Phys.*, 2012, **86**, 021507.
14 P. Mansky, J. DeRouchey, T. P. Russell, J. Mays, M. Pitsikalis, T. Morkved and H. Jaeger, *Macromolecules*, 1998, **31**, 4399.
15 V. Olszowka, L. Tsarkova and A. Böker, *Soft Matter*, 2009, **5**, 812.

16 Y. Tao, H. Zohar, B. D. Olsen and R. A. Segalman, *Nano Lett.*, 2007, **7**, 2742.
17 S. Pujari, M. A. Keaton, P. M. Chaikin and R. A. Register, *Soft Matter*, 2012, **8**, 5358.
18 B. C. Berry, A. W. Bosse, J. F. Douglas, R. L. Jones and A. Karim, *Nano Lett.*, 2007, **7**, 2789.
19 I. Bita, J. K. W. Yang, Y. S. Jung, C. A. Ross, E. L. Thomas and K. K. Berggren, *Science*, 2008, **321**, 939.
20 E. Kim, H. Ahn, S. Park, H. Lee, M. Lee, S. Lee, T. Kim, E.-A. Kwak, J. H. Lee, X. Lei, J. Huh, J. Bang, B. Lee and D. Y. Ryu, *ACS Nano*, 2013, **7**, 1952.
21 Y. Tada, S. Akasaka, M. Takenaka, H. Yoshida, R. Ruiz, E. Dobisz and H. Hasegawa, *Polymer*, 2009, **50**, 4250.
22 Y. S. Jung, W. Jung and C. A. Ross, *Nano Lett.*, 2008, **8**, 2975.
23 M. P. Stoykovich, H. Kang, K. C. Daoulas, G. Liu, C.-C. Liu, J. J. de Pablo, M. Müller and P. F. Nealey, *ACS Nano*, 2007, **1**, 168.
24 M. Luo and T. H. Epps III, *Macromolecules*, 2013, **46**, 7567.
25 J. W. Park and Y. H. Cho, *Langmuir*, 2006, **22**, 10898.
26 W. Xu, Z. Xu, C. Cai, J. Lin, S. Zhang, L. Zhang, S. Lin, Y. Yao and H. Qi, *J. Phys. Chem. Lett.*, 2019, **10**, 6375.
27 M. H. M. Cativo, D. K. Kim, R. A. Riggleman, K. G. Yager, S. S. Nonnenmann, H. Chao, D. A. Bonnell, C. T. Black, C. R. Kagan and S.-J. Park, *ACS Nano*, 2014, **8**, 12755.
28 S. Oh, M. Yang, S. Kang, S.-H. Chung, J. Bouffard, S. Hong and S.-J. Park, *ACS Appl. Mater. Interfaces*, 2019, **11**, 28538.
29 S. Oh, S. Kang, M. H. M. Cativo, M. Yang, S.-H. Chung, J. Kim, J. Bouffard, S. Hong and S.-J. Park, *ACS Appl. Mater. Interfaces*, 2020, **12**, 509.
30 J. W. Park and E. L. Thomas, *J. Am. Chem. Soc.*, 2002, **124**, 514.
31 S. M. Jeong, M. Song and J. W. Park, *Soft Matter*, 2012, **8**, 1309.
32 M. Han, M. S. Rahman, J.-S. Lee, D. Khim, D.-Y. Kim and J.-W. Park, *Chem. Mater.*, 2011, **23**, 3517.
33 J. W. Park, H. Kim and M. Han, *Chem. Soc. Rev.*, 2010, **39**, 2935.
34 A. Cavallo, M. Müller and K. Binder, *Macromolecules*, 2008, **41**, 4937.
35 J. F. Douglas, H. E. Johnson and S. Granick, *Science*, 1993, **262**, 2010.
36 P. J. Hoogerbrugge and J. M. V. A. Koelman, *Europhys. Lett.*, 1992, **19**, 155.
37 P. Español and P. Warren, *Europhys. Lett.*, 1995, **30**, 191.
38 Q. Li, L. Wang, J. Lin and L. Zhang, *Phys. Chem. Chem. Phys.*, 2019, **21**, 2651.
39 R. D. Groot and P. B. Warren, *J. Chem. Phys.*, 1997, **107**, 4423.
40 X. Ye, Z. Li, Z. Sun and B. Khomami, *ACS Nano*, 2016, **10**, 5199.
41 X. Zhang, L. Wang, L. Zhang, J. Lin and T. Jiang, *Langmuir*, 2015, **31**, 2533.
42 Q. Li, L. Wang and J. Lin, *Phys. Chem. Chem. Phys.*, 2017, **19**, 24135.
43 M. W. Matsen, *J. Chem. Phys.*, 2001, **114**, 10528.
44 J. V. Selinger and R. F. Bruinsma, *J. Phys. II*, 1992, **2**, 1215.
45 Z. Li, W. Zhao, Y. Liu, M. H. Rafailovich, J. Sokolov, K. Khougaz, A. Eisenberg, R. B. Lennox and G. Krausch, *J. Am. Chem. Soc.*, 1996, **118**, 10892.
46 S. Roland, C. G. Gamys, J. Grosrenaud, S. Boissé, C. Pellerin, R. E. Prud'homme and C. G. Bazuin, *Macromolecules*, 2015, **48**, 4823.
47 S. Roland, D. Gaspard, R. E. Prud'homme and C. G. Bazuin, *Macromolecules*, 2012, **45**, 5463.
48 P. Espanol and P. Warren, *J. Chem. Phys.*, 2017, **146**, 150901.
49 W. G. Noid, *J. Chem. Phys.*, 2013, **139**, 090901.
50 Z. Qiang, L. Zhang, G. E. Stein, K. A. Cavicchi and B. D. Vogt, *Macromolecules*, 2014, **47**, 1109.
51 Z. Lin, D. H. Kim, X. Wu, L. Boosahda, D. Stone, L. Larose and T. P. Russell, *Adv. Mater.*, 2002, **14**, 1373.
52 K. Yue, C. Liu, M. Huang, J. Huang, Z. Zhou, K. Wu, H. Liu, Z. Lin, A.-C. Shi, W.-B. Zhang and S. Z. D. Cheng, *Macromolecules*, 2017, **50**, 303.
53 C. M. Bates, T. Seshimo, M. J. Maher, W. J. Durand, J. D. Cushen, L. M. Dean, G. Blachut, C. J. Ellison and C. G. Willson, *Science*, 2012, **338**, 775.
54 L.-Y. Shi, S. Lee, L.-C. Cheng, H. Huang, F. Liao, R. Ran, K. G. Yager and C. A. Ross, *Macromolecules*, 2019, **52**, 679.
55 V. Pryamitsyn and V. Ganesan, *J. Chem. Phys.*, 2004, **120**, 5824.
56 T. Thurn-Albrecht, J. Schotter, G. A. Kästle, N. Emley, T. Shibauchi, L. Krusin-Elbaum, K. Guarini, C. T. Black, M. T. Tuominen and T. P. Russell, *Science*, 2000, **290**, 2126.
57 J. I. Lee, S. H. Cho, S.-M. Park, J. K. Kim, J. K. Kim, J.-W. Yu, Y. C. Kim and T. P. Russell, *Nano Lett.*, 2008, **8**, 2315.
58 M. Park, C. Harrison, P. M. Chaikin, R. A. Register and D. H. Adamson, *Science*, 1997, **276**, 1401.
59 Y. S. Jung and C. A. Ross, *Nano Lett.*, 2007, **7**, 2046.
60 E. Fredenberg, M. Lundqvist, B. Cederström, M. Åslund and M. Danielsson, *Nucl. Instrum. Methods Phys. Res., Sect. A*, 2010, **613**, 156.